Water Research 95 (2016) 134–141

Contents lists available at ScienceDirect

Water Research

journal homepage: www.elsevier.com/locate/watres

Novel application of nanozeolite for radioactive cesium removal from high-salt wastewater

Keun-Young Lee*, Kwang-Wook Kim, Minsung Park, Jimin Kim, Maengkyo Oh, Eil-Hee Lee, Dong-Yong Chung, Jei-Kwon Moon

Korea Atomic Energy Research Institute (KAERI), 989-111 Daedeok-daero, Yuseong-gu, Daejeon, 305-353, Republic of Korea

ARTICLE INFO

Article history:
Received 22 December 2015
Received in revised form
24 February 2016
Accepted 24 February 2016
Available online 26 February 2016

Keywords:
Nanoadsorbent
Radioactive cesium
Chabazite
Adsorption
Flocculation

ABSTRACT

Finding a striking peculiarity of nanomaterials and evaluating its feasibility for practical use are interesting topics of research. We investigated the application of nanozeolite's outstanding reactivity for a rapid and effective method for radioactive cesium removal in the wastewater generated from nuclear power plant accident, as a new concept. Extremely fast removal of cesium, even without stirring, was achieved by the nanozeolite at efficiencies never observed with bulk materials. The nanozeolite reached an adsorption equilibrium state within 1 min. Cesium adsorption by nanozeolite was demonstrated at reaction rates of orders of magnitude higher than that of larger zeolite phases. This observation was strongly supported by the positive correlation between the rate constant ratio ($k_{2,bulk}/k_{2,nano}$) and the initial Cs concentrations with a correlation coefficient (R^2) of 0.99. A potential drawback of a nanoadsorbent is the difficulty of particle settling and separation because of its high dispersivity in solution. However, our results also demonstrated that the nanozeolite could be easily precipitated from the high-salt solution with ferric flocculant. The flocculation index reached a steady state within 10 min. A series of our experimental results met the goal of rapid processing in the case of emergency by applying the well-suited nanozeolite adsorption and flocculation.

1. Introduction

The treatment of wastewater containing radionuclides has become one of the most significant challenges facing the nuclear industry, which was highlighted from the generation of a large volume of radioactive wastewater and its release into surrounding soil, groundwater, and seawater after the severe accident at Fukushima, Japan in 2011 (ANS, 2012; Kosaka et al., 2012). Because high-salt and high-level radioactive wastewater in large quantities can be generated after emergency cooling the damaged reactors, a problem was caused by several small and large leakages of wastewater from the treatment system and storage tanks that were hurriedly installed in the early stages of the incident (ANS, 2012; TEPCO, 2012a). Therefore, to minimize the storage of wastewater and release of radionuclides into the environment, a novel emergency treatment system capable of rapid, effective, and convenient operation is required, followed by recycling of treated water back into the reactors.

Radioactive cesium is the most crucial and problematic element of the radionuclides because of its abundance in the target wastewater and the hazards presented by its high specific radioactivity and long half-life (Dubourg, 1998; TEPCO, 2012b). Although there are a number of methods for purifying the waste solutions, ion exchange and adsorption have been considered to be the most effective methods for removal of radioactive cesium from the high-salt and high-level radioactive wastewater. The method is the most effective because the chemical concentration of cesium is relatively low despite its high radioactivity, whereas the concentrations of background ions are high (Dubourg, 1998). The major existing on-site wastewater treatment system at Fukushima site is also based on cesium adsorption by column operation using zeolites as the adsorbent (Sylvester et al., 2013). Zeolites or zeolitic materials have been preferred over organic materials for the treatment of high-level radioactive liquid waste because of their radiological and thermal stability as inorganic adsorbents (Plazinski and Rudzinski, 2009).

Nanoadsorbent-based wastewater treatment offers a promising approach to overcome current drawbacks and provide outstanding

* Corresponding author.
E-mail address: lky@kaeri.re.kr (K.-Y. Lee).

http://dx.doi.org/10.1016/j.watres.2016.02.052
0043-1354/

performances on the contaminant removal from wastewater in many different industrial applications (Qu et al., 2013). Nanomaterials have extremely high specific surface areas, adsorption sites, and reactivity, whereas conventional bulk materials have chemical and biogeochemical limitations in terms of surface area, active sites, and reaction kinetics (Sharma et al., 2009; Bosch et al., 2012; Qu et al., 2013). Research on nanozeolite has focused on chemical sensors, thin films, enhanced catalysts, and macrostructure composite materials (Hedlund et al., 1997; Choi et al., 2000; Pan et al., 2009; Serrano et al., 2009). In wastewater treatment applications, nanozeolite has been used in membrane processes for the removal of metal ions, where the main goal is to increase the hydrophilicity of the membrane (Jawor and Hoek, 2010; Pendergast and Hoek, 2011). A few studies have investigated water treatment using nanoadsorbent in powder form in slurry reactors with an additional separation unit to recover the nanoparticles (Sharma et al., 2009; Qu et al., 2013), although the minute particle of the nanoadsorbent size poses a challenge. In the same manner, a number of advantages of nanomaterials, especially nanozeolites, need to be explored in various fields of scientific research. To the best of our knowledge, although interests in the various applications of nanoadsorbents including nanozeolite have been attracting growing interest, there has been no research on the use of nanozeolite in the treatment of radioactive wastewater. Moreover, a precipitation method based on adsorption–flocculation mechanisms offers a promising design approach to an emergency treatment system. In this study, the cesium adsorption properties of nanochabazite (a form of zeolite) were determined and compared to those of bulk chabazite. A feasibility study on the application of the adsorption–flocculation process was also conducted in a real environmental setting where radioactive contamination by cesium was present.

2. Experimental section

2.1. Chabazite

Four types of chabazite were used for this study. A commercially available chabazite, AW500 manufactured by Linde (Sigma–Aldrich, Molecular sieve, 1.6 mm pellet) was used for comparison with pure synthesized chabazite. The AW500 pellet was ground and sieved to less than 212 μm to produce AW500-powder. Pure chabazite was synthesized from the decomposition of a commercial grade of zeolite Y (Sigma–Aldrich, LZ-Y62, powder) following the method suggested by Bourgogne et al. (1985). Moreover, 99.1 mL of deionized water (Millipore, Direct-Q 3) was mixed with 13.4 mL of 45 wt% potassium hydroxide solution, and 12.5 g of zeolite Y was added to the mixture and shaken for 30 s in a polypropylene bottle (250 mL, Nalgene). The batch composition of the gel was 0.17 Na_2O:2.0 K_2O:Al_2O_3:5.18 SiO_2:224 H_2O. The gel was then placed in an oven at 368 K for 4 days. The products were washed by deionized water with sonication and dried in an oven at 333 K for more than 48 h. The product synthesized by this procedure shows submicron crystallites with hundreds of nanometers (Bourgogne et al., 1985). For the synthesis of micro-sized chabazite (CHA-micro), the existing method for nanochabazite (CHA-nano) production was modified in this study. The batch composition and mixture conditions were identical to those in the procedure already described. However, the synthesis temperature was decreased to 358 K, and the crystallizing period was increased to 14 days. All the prepared chabazites were then ion exchanged to the sodium form using 1 M NaCl solution at 333 K with a solution comprising chabazite ratio of 50 mL/g in eight ion exchange cycles, each lasting more than 9 h. This yielded sodium-exchanged chabazites (Smith et al., 2001; Ridha et al., 2009).

2.2. Characterization of chabazite

The particle sizes of the prepared chabazites were determined on the basis of particle dispersibility in deionized water. CHA-nano was a very stable colloidal phase in solution; therefore, the mean volume diameter of the colloidal sample could be measured by dynamic light scattering (DLS; Malvern ZS90, UK), which allowed exact determination of the nanometer size of particles dispersed in the solution. Conversely, the CHA-micro and AW500-powder were measured by laser diffraction (LD; Microtrac S3500, Japan), because most of the particles settled to the bottom. This gave a detection range of 0.7–1000 μm in a fluidized solution condition.

Powder X-ray diffraction (XRD; Bruker D2 Phaser, Germany) was used for identification of the prepared chabazites. Particle morphology and size were examined by scanning electron microscopy (SEM; SEC SNE-4500M, Korea).

2.3. Batch adsorption tests

The sample solutions for the batch adsorption experiments were prepared by dissolving cesium chloride (Sigma–Aldrich, CsCl 99.9%) in seawater collected from the Korean East Sea with initial Cs concentrations of 100 and 10 mg/L for the nonradioactive experiments, and 1 mg/L and 1 μg/L with ^{137}Cs as a tracer level for the radioactive experiments. The seawater was used after filtration, and it had initial Na and Cl concentrations of 10675 and 19700 mg/L, respectively, as well as a range of other ions including Ca, K, Mg, Br, and SO_4. This was considered as a Cs contaminated condition with high-salt content. Adsorption experiments were conducted for different m/Vs (g-chabazite/L) under shaking or static conditions for 2 h at room temperature. All experiments were repeated in triplicate, and running blanks were measured for experimental accuracy. After the experiments, the samples were collected by filtering supernatants through a 0.2 μm membrane (Advantec, DISMIC-13) and diluted with deionized water to form appropriate concentrations prior to analysis by atomic absorption spectroscopy (AAS; PerkinElmer AAnalyst 900F, USA) and inductively coupled plasma-mass spectrometry (ICP-MS; PerkinElmer Elan DRC ii, USA) for the nonradioactive samples and multi channel analyzer (MCA; Oxford TC702, UK) for radioactive samples. To ignore the matrix effect on Cs in the AAS analysis of the seawater samples, a constant level of seawater-based standard solution was used. The Cs adsorption results are given as adsorption yields (A, %) and distribution coefficients (K_d, mL/g) and are based on the following equations:

$$A = \frac{(C_i - C_f)100}{C_i} \quad (1)$$

$$K_d = \frac{(C_i - C_f)1000V}{C_f m} \quad (2)$$

where C_i (mg/L) is the initial Cs concentration, C_f (mg/L) is the final Cs concentration from the supernatant solution, V (L) is the solution volume, and m (g) is the mass of chabazite used. The Cs adsorption capacity (q, mg/g) of chabazites with m/V = 1 (1 g-chabazite/L dose) for 2 h was calculated from the mass balance as follows:

$$q = \frac{(C_i - C_f)V}{m} \quad (3)$$

2.4. Kinetic studies

Samples were collected at appropriate time intervals from the batch adsorption experiments to investigate the adsorption kinetics. The pseudo second-order kinetic model was applied to analyze the adsorption processes expressed as follows:

$$q_t = \frac{k_2 q_e t}{1 + k_2 q_e t} \quad (4)$$

where t (min) is the contact time, k_2 (g/mg min) is the adsorption rate constant, and q_t and q_e (mg/g) are the adsorption capacity of Cs at time t and equilibrium, respectively. The values of q_e and k_2 were determined experimentally from the intercept and slope of a plot of t/q_t versus t (Ho and McKay, 1998; Reddad et al., 2002). The rate constants of the nanosized and bulk chabazites were used to evaluate the kinetic properties by plotting the ratio of these constants against initial Cs concentrations.

2.5. Thermodynamic studies

To compare the thermodynamic properties of the adsorption processes of nanosized and bulk chabazites, CHA-nano and AW500-powder were added to the sample solution at an initial Cs concentration of 100 mg/L with a chabazite dose of 1 g/L at three temperatures (301 K, 309 K, and 318 K) for 4 h. Standard enthalpy (ΔH°) and standard entropy (ΔS°) changes were determined from the slope and intercept of the linear function by plotting $\ln K_d$ against 1/T, respectively, and standard Gibbs free energy (ΔG°) was calculated by the following:

$$\ln K_d = \frac{\Delta S^o}{R} - \frac{\Delta H^o}{RT} \quad (5)$$

$$\Delta G^o = \Delta H^o - T\,\Delta S^o \quad (6)$$

where K_d (mL/g) is the distribution coefficient, R (8.314 J/mol K) is the gas constant, and T (K) is the absolute temperature of the aqueous solution (Tsai et al., 2009; Nilchi et al., 2011).

2.6. Activation energy

The activation energy (E_a) of adsorption was calculated from the Arrhenius equation, which represents the minimum energy for the adsorption reaction:

$$\ln k_2 = \ln A - \frac{E_a}{RT} \quad (7)$$

where k_2 (g/mg min) is the rate constant obtained from the pseudo second-order equation, A is the Arrhenius factor, E_a (kJ/mol) is the activation energy of adsorption. E_a can be determined through the linear plots of $\ln k_2$ against 1/T (Ahn and Iton, 1991; Mahmoud et al., 2012).

2.7. Flocculation of nanochabazite

The dispersion property of the nanosized chabazite was evaluated by measuring the light transmission (%) of the colloidal sample (m/V = 5 g-chabazite/L) dispersed in deionized water, seawater, and NaCl solutions at various concentrations under static conditions for 2 h. A liquid dispersion optical analyzer using a pulsed near-infrared light source ($\lambda = 850$ nm; Formulation Turbiscan Lab, France) was used to determine the percentage of light transmission by vertical scanning across the height of the sample in a cylindrical glass cell over time (Mengual et al., 1999). To evaluate the kinetics of nanoparticle flocculation in the sample solutions, the flocculation index (FI) was represented by calculating the ratio between the transmission data of the dispersion sample and each blank sample as follows:

$$FI = \frac{T_s}{T_b} \quad (8)$$

where T_s and T_b (%) are the percentages of light transmitted through the samples and blanks, respectively. The variation in the flocculation index of the nanosized chabazite was also monitored with and without the injection of the inorganic flocculant, ferric iron (Fe^{3+}; Sigma–Aldrich, $FeCl_3$), by 0.1–1 g-Fe/L doses with adjustment using a suitable amount of 1 M sodium hydroxide solution to neutral pH in the seawater. The particle morphology and size changes in different solution conditions were observed using a video microscope system (Sometech IcamScope, Korea). The zeta potentials of the nanochabazite in deionized water and seawater were measured using a zeta potential analyzer (Malvern ZS90, UK).

3. Results and discussion

3.1. Characterization of chabazite

The crystallinities of the synthesized and commercial chabazites were confirmed by X-ray diffraction. Although the commercial AW500 contained a small amount of impurities such as clay that is used as a pelletizing reagent, the XRD peaks obtained from all the chabazite samples occurred precisely at their theoretically predicted positions. SEM images of the synthesized and commercial chabazites used in the Cs adsorption experiments are shown in Fig. 1, and their mean particle sizes are presented in Table 1. The particles of CHA-nano appeared as an aggregated complex with nanosized chabazite crystals. The particle size of the CHA-nano measured by DLS demonstrated a mean value of 510.7 nm with a size distribution in the range of several hundred nanometers. The mean particle size of the CHA-micro (12.9 μm) was larger than that of CHA-nano. This was a result of the formation of rod-shaped chabazite crystals of micrometer lengths (Fig. 1B). In general, the size and shape of a crystal depends on the reaction rate and is affected by a range of synthesis parameters including gel composition, degree of reactant saturation, temperature, and aging (Cundy and Cox, 2005; Subotic and Bronic, 2003). A slow reaction rate favors the formation of large crystals and is used to give a direction to the growth of the crystal when the degree of saturation and temperature are relatively low (Sangwal, 2007; Kim et al., 2015). Because the gel composition in the synthesis of the pure chabazite was fixed, lower temperatures and longer times than normal were applied to increase the size of the crystals grown. At 358 K, it was found that no pure chabazite was synthesized earlier than 14 days (data not shown). The particle shapes of the AW500-powder were not uniform, and the mean particle size was 128.9 μm. The raw material used was a pellet type chabazite with a length of >1 mm. These results demonstrated that the chabazite samples could be prepared with the same zeolite type and different particle sizes.

3.2. Cs adsorption properties of nanochabazite

The adsorption yields of Cs and distribution coefficients of the four types of chabazite with different m/V in seawater containing Cs at 100 mg/L are shown in Fig. 2A. There was no significant difference between the Cs adsorption efficiency of the CHA-nano and the CHA-micro, although both were somewhat higher in efficiency

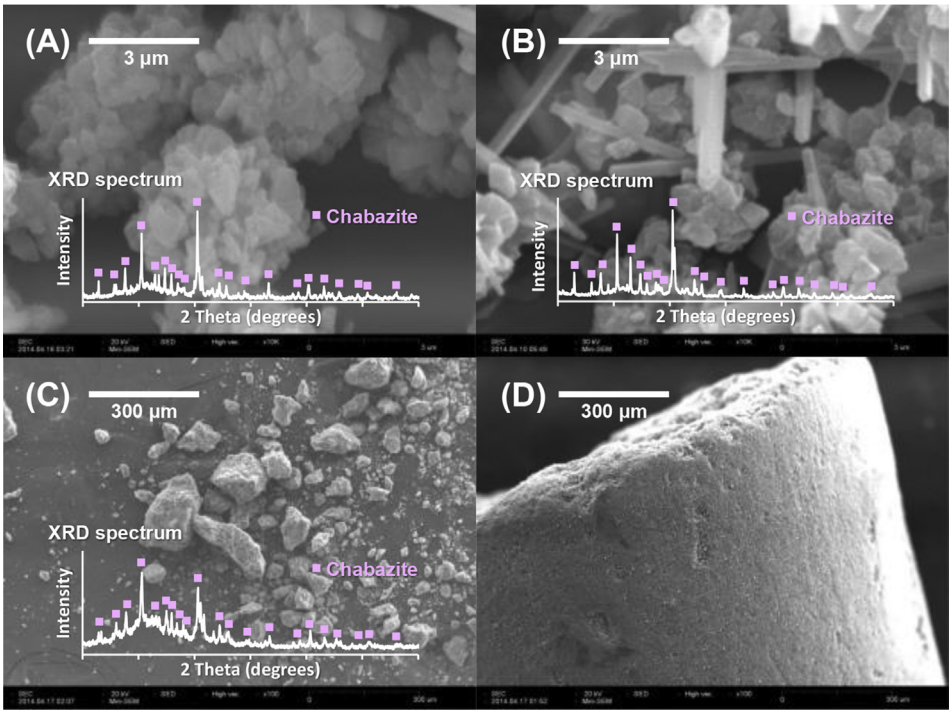

Fig. 1. SEM images and XRD spectra of (A) CHA-nano, (B) CHA-micro, (C) AW500-powder, and (D) AW500-pellet used for Cs adsorption experiments. XRD spectrum of AW500-pellet does not differ from that of AW500-powder. Obtained X-ray diffraction peaks exactly occur at the theoretically expected positions (■).

Table 1
Mean particle sizes of chabazites measured by different methods.

	Type	LD[c]	DLS[d]	SEM[e]
CHA-nano	Pure chabazite[a]	–	510.7 ± 63 nm	<5 μm
CHA-micro	Pure chabazite	12.9 ± 2.5 μm	–	<20 μm
AW500-powder	Ground powder[b]	128.9 ± 4.4 μm	–	<200 μm
AW500-pellet	Commercial chabazite pellet	–	–	>1 mm

[a] Synthesized by hydrothermal method.
[b] Commercial chabazite pellet was ground and sieved under 212 μm.
[c] Mean volume diameter of sample in fluidized condition measured by LD (laser diffraction).
[d] Mean volume diameter of static colloidal sample by DLS (dynamic light scattering).
[e] Observation of dried sample by SEM (scanning electron microscopy).

than the AW500-powder, especially when the m/V ratio was small. As shown in Fig. 2B, the Cs adsorption capacity of the AW500-powder was only three quarters of that of the pure chabazites at 1 g-chabazite/L doses. Because the commercialized chabazite comprises both chabazite crystals and specific pelletizing agents, the inert pelletizing agents are expected to reduce the mass based cesium adsorption capacity of that material. The Cs adsorption efficiency of the AW500-pellet was significantly lower than that of the other samples. This strongly suggests that the diffusion and adsorption of Cs in the pellet is reduced by the impurities, delaying or decreasing Cs adsorption. To confirm that the Cs adsorption rate depended on the particle size, changes in the Cs adsorption capacities over time were observed and the adsorption kinetics were analyzed using a pseudo second-order kinetic model (Fig. 3). The CHA-nano reached adsorption equilibrium within 1 min, the first sampling point in the experiment (Fig. 3A). This result provides clear evidence that the Cs adsorption of nanochabazite is extremely fast even in seawater. The adsorption rate decreased as the particle size increased, which was reflected not only in the time required to reach adsorption equilibrium but also the rate constant calculated from the kinetic model (Fig. 3B). The rate constant of the CHA-nano was larger than that of the CHA-micro; moreover, the rate constant of the AW500-powder was larger than that of the AW500-pellet. The Cs adsorption rate of bulk zeolites in the range of several hundred micrometers has been thoroughly investigated in previous studies (Mimura and Kanno, 1985). Our results show that the reaction rate of nanozeolite is much faster than that of bulk zeolite. In emergencies, such as an accident at a nuclear power plant, rapid processing and treatment of the radioactive wastes is essential. In such contexts, nanochabazite offers a much faster way of removing the radioactive Cs from the wastewater and recycling the treated water as a reactor coolant.

Fig. 4 shows the kinetics of Cs adsorption by chabazites with 10 g-chabazite/L of m/V under both shaken and static conditions. In the case of the CHA-nano, no significant difference was found in the Cs adsorption rate or Cs adsorption capacity when shaken and static (see Fig. 2 and the inset box in Fig. 4B). Conversely, the efficiencies of the other chabazite samples were significantly lower when static than when shaken. The small particle size of the CHA-nano allowed it to disperse fully in the solution immediately after injection, whereas the other chabazite types settled out of solution before the completion of Cs adsorption. The nanochabazite therefore offers significant advantages for Cs removal under conditions where stirring is not possible.

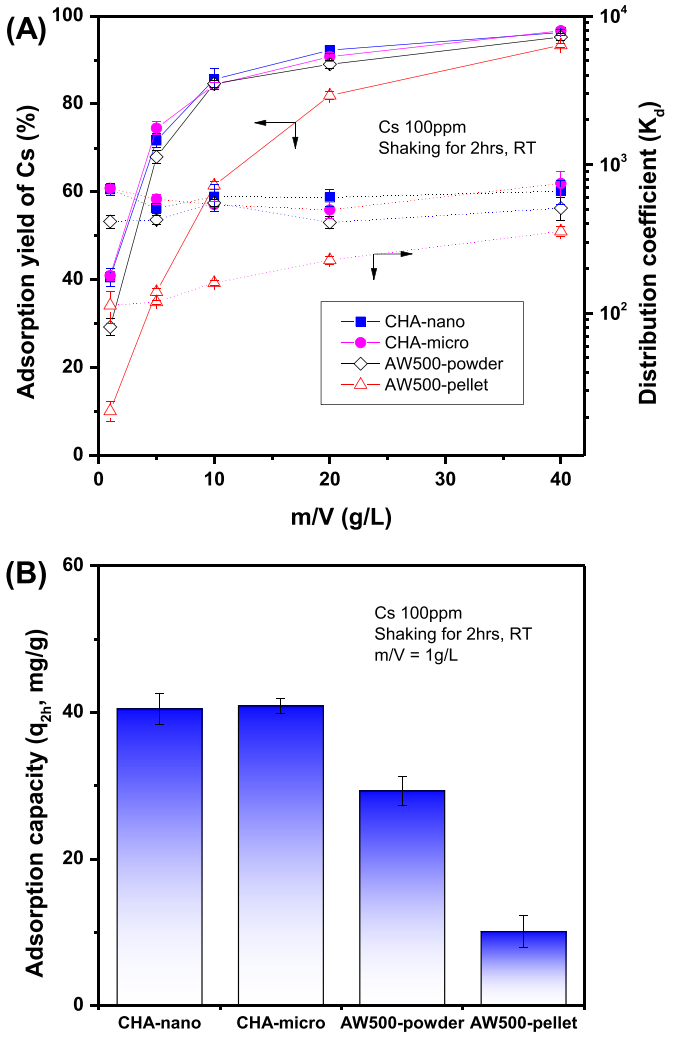

Fig. 2. (A) Adsorption yield% of Cs and distribution coefficients of chabazites with different m/V and (B) Cs adsorption capacities of them with 1 g-chabazite/L of m/V after shaking for 2 h in seawater containing Cs 100 mg/L.

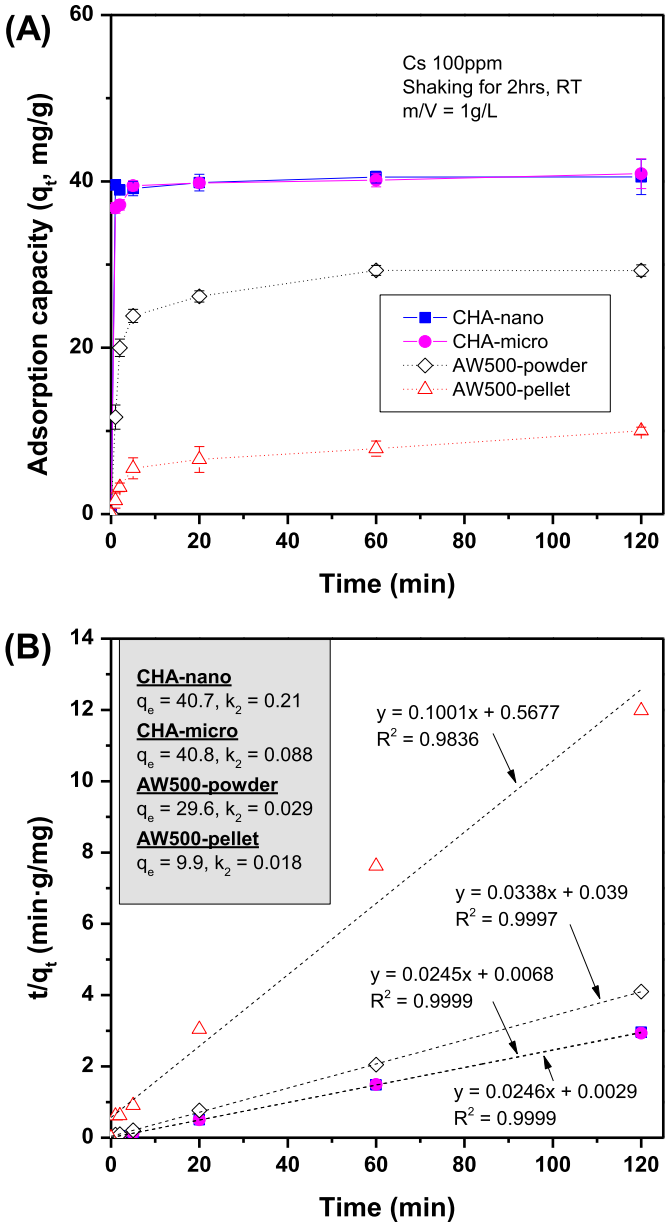

Fig. 3. (A) Variations of Cs adsorption capacities with time and (B) kinetic analyses by pseudo second-order reaction model of chabazites with 1 g-chabazite/L of m/V after shaking for 2 h in seawater containing Cs 100 mg/L. The equilibrium adsorption capacities (q_e) and the adsorption rate constants (k_2) of chabazites calculated from the kinetic model were represented in the inset box.

The thermodynamic parameters and activation energies were derived by plotting straight lines of $\ln K_d$ and $\ln K_2$, respectively, versus 1/T with a correlation coefficient (R^2) of 0.99 (Fig. 5). The thermodynamic parameters of the CHA-nano and AW500-powder are shown in the inset box of Fig. 5A. The distribution coefficient of Cs adsorption by both chabazites decreased as the temperature increased, indicating that they were favorable for Cs adsorption at low temperatures. The negative ΔG° at different temperatures and ΔH° showed that Cs adsorption by both chabazites was a spontaneous and exothermic reaction. The activation energies calculated from the Arrhenius equation were higher than 40 kJ/mol (inset box of Fig. 5B), implying that the reaction was a chemical adsorption with stable bonding of Cs in the chabazite structure. These adsorption properties when analyzed by the reaction phenomena showed no significant differences between the nano and bulk chabazites. This confirms that the particle size at the nanoscale affects only the adsorption rate of Cs and has no effect on the number of adsorption sites or thermodynamic reactions. The bulk solution diffusivity of the Cs ion is much faster than its intraparticle diffusivity in the zeolite, which is the main reason that the Cs adsorption rate was determined primarily by the solution diffusivity when the same amount of zeolite was introduced as extremely small particle in the solution. The combination of the rapid particle dispersion in solution and the rapid Cs adsorption of the nanozeolite led the reaction to equilibrium within 1 min under both shaken and static experimental conditions.

3.3. Nano chabazite in radioactive wastewater

As aforementioned, the actual level of Cs concentration in waste seawater following an accident like that at Fukushima may be less than 1 mg/L, even if the radioactivity level of the Cs is high (TEPCO, 2011). To closely simulate a real accident, comparative experiments were conducted using sample solutions containing initial Cs concentrations of 1 mg/L and 1 μg/L with ^{137}Cs as a tracer level. Fig. 6 shows the adsorption yields of Cs and the distribution coefficients

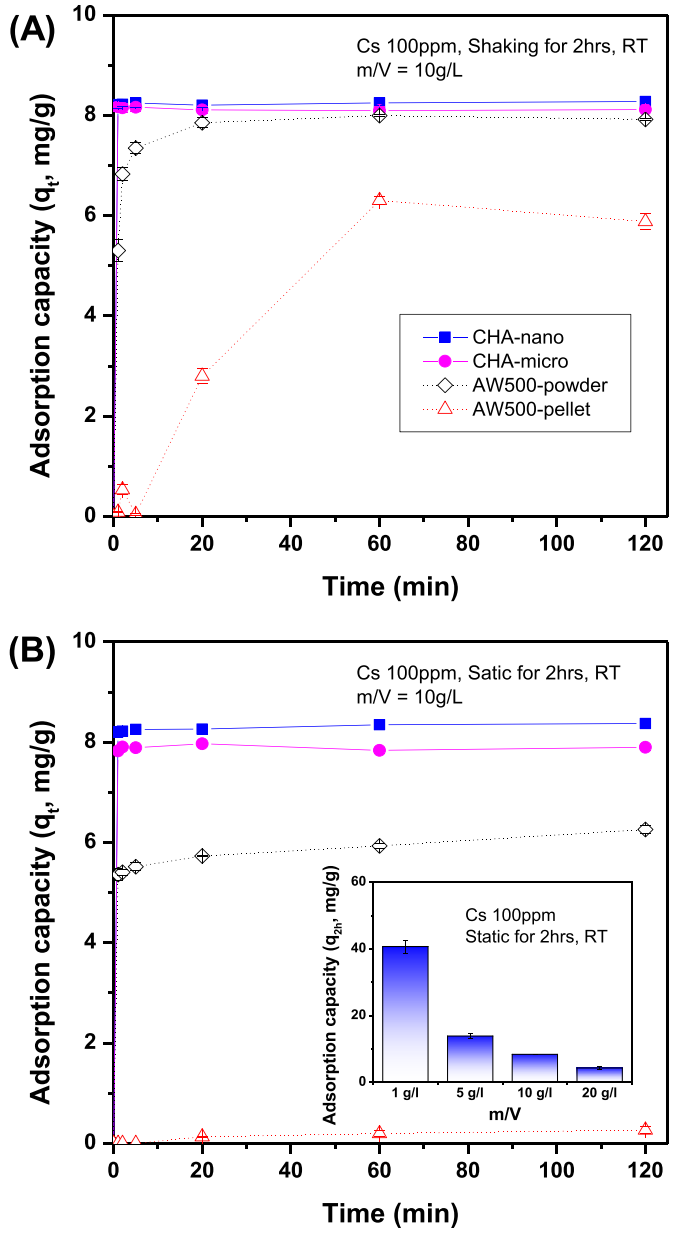

Fig. 4. Variations of Cs adsorption capacities of chabazites with time in (A) shaking and (B) static conditions for 2 h with 10 g-chabazite/L of m/V in seawater containing Cs 100 mg/L (Inset box: Cs adsorption capacities of CHA-nano in static conditions for 2 h with different m/V).

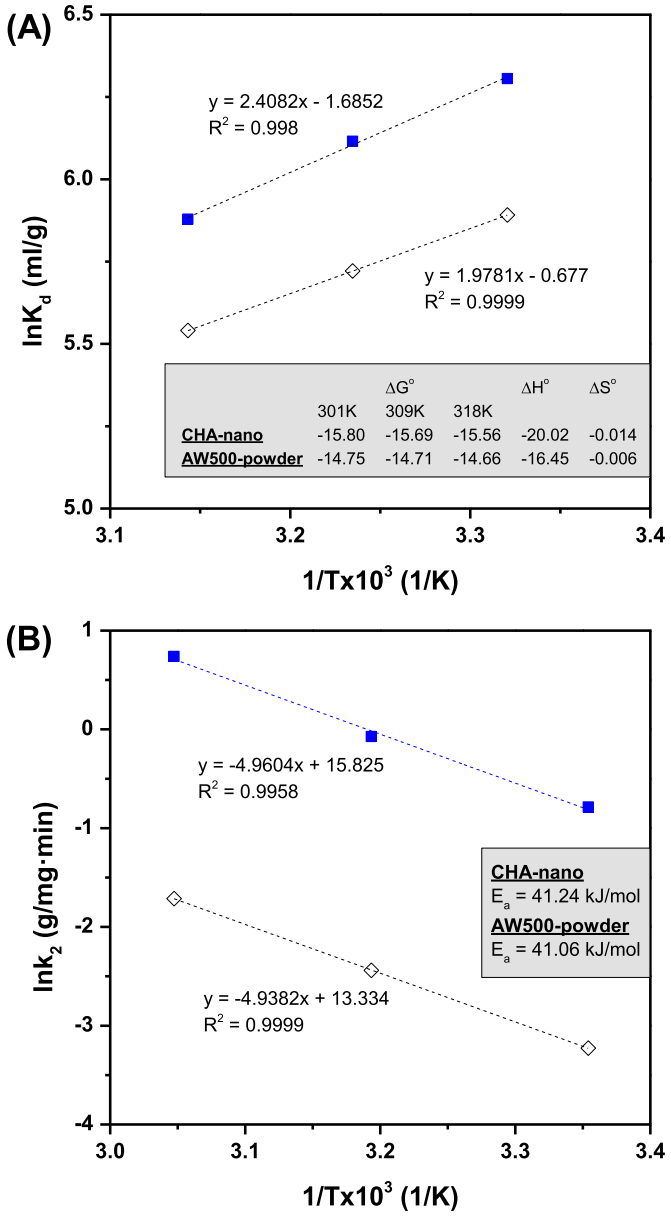

Fig. 5. (A) Thermodynamic parameters and (B) activation energies of CHA-nano and AW500-powder (unit: kJ/mol) obtained from Cs adsorption experiments in seawater containing Cs 100 mg/L.

of CHA-nano and AW500-powder with different m/Vs in seawater containing 1 mg/L and 1 μg/L of Cs. The overall Cs adsorption efficiency was not significantly different in the low initial concentration conditions and the high initial concentration conditions (See Figs. 2A and 6A). Moreover, the tendency of Cs adsorption rates of the nano and bulk chabazites were not different under those conditions. The nanochabazite reached an adsorption equilibrium state within 1 min, almost immediately after injection (See Fig. 3A and inset box of 6B). However, the difference in the Cs adsorption rates of the nano and bulk chabazites was greater at lower initial Cs concentrations. This observation was strongly supported by the positive correlation between the rate constant ratio between them ($k_{2,bulk}/k_{2,nano}$) and the different initial Cs concentrations with a correlation coefficient (R^2) of 0.99 (Fig. 6B). Bulk chabazite required a longer time to reach an equilibrium state at low Cs concentrations. However, there was no difference in the adsorption rate of nanochabazite at the different initial concentrations of Cs. Therefore, rapid removal of Cs by nanochabazite could be even more pronounced under the actual conditions of an incident involving radioactive wastewater.

3.4. Flocculation of nanochabazite

Because the flocculation index represents the ratio between the percentage of light transmitted through the dispersion sample and a blank sample, the index of ideal flocculation is close to 1. In Fig. 7A, the flocculation rates of CHA-nano in different solution conditions were compared by plotting the flocculation indices over time. The flocculation rate of nanochabazite in seawater was much faster than that in deionized water. The flocculation of nanoparticles without the addition of flocculant, known as self-

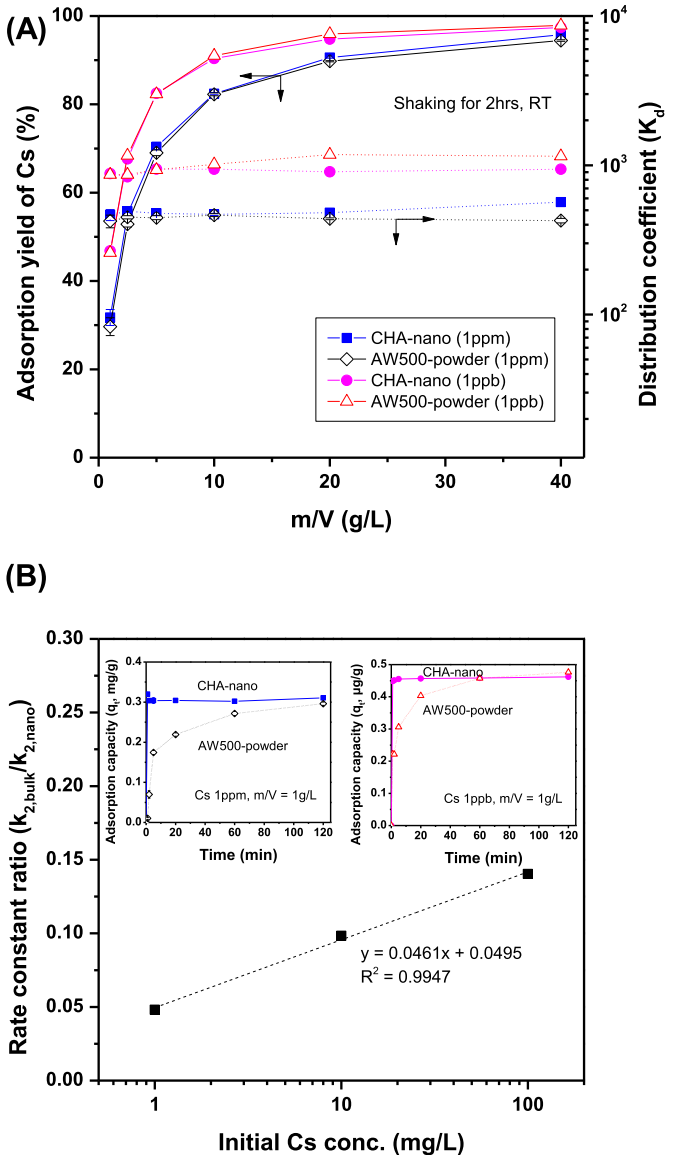

Fig. 6. (A) Adsorption yield% of Cs and distribution coefficients of CHA-nano and AW500-powder with different m/V and (B) correlation between rate constant ratio and initial Cs concentration of them with shaking 1 g-chabazite/L of m/V for 2 h in seawater (Inset box: Variations of Cs adsorption capacities of them with time at Cs 1 μg/L and 1 mg/L with 1 g-chabazite/L).

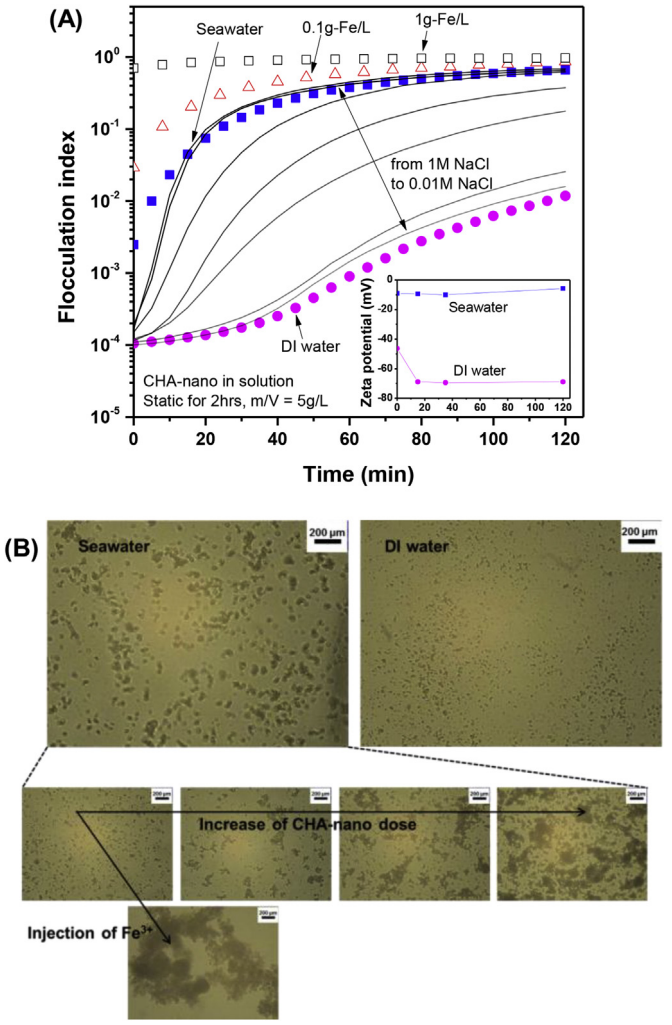

Fig. 7. (A) Variations of flocculation index of CHA-nano with time in deionized water, solutions with different NaCl concentrations, seawater with and without Fe coagulant in static conditions measured by Turbiscan (Inset box: variations of zeta potential of CHA-nano with time in seawater and deionized water) and (B) microphotographs of CHA-nano in different conditions.

flocculation, could be explained by destabilization of the particle in the high-salt conditions (Bratby, 2006). As shown in the inset box of Fig. 7A, the absolute values of the zeta potential of nanochabazite in seawater were much lower than those in deionized water, implying that the dispersion stability of nanochabazite could be markedly decreased in seawater. Moreover, the flocculation rate dramatically increased as the NaCl concentration was increased from 0.01 to 1 M. Although the nanoadsorbent has a drawback in terms of the difficulty of particle settling and separation because of its small particle size and high dispersion stability, our results demonstrated that the nanoadsorbent could be easily precipitated from the waste seawater immediately after Cs adsorption. In the experiments using the additional inorganic flocculant, ferric iron, the flocculation rate of the nanochabazite in seawater increased and the flocculation index of the 1 g-Fe/L dose reached a steady state within 10 min. Fig. 7B shows the morphology and size changes of the CHA-nano in different solution conditions. The destabilized chabazite particles in seawater were observed to be much larger than those in deionized water, and the flocculation reaction was significantly enhanced when the particle dosage was increased and the Fe flocculant was injected. The results demonstrate that it is possible to reduce the settling time and increase the floc size of nano-chabazite by injecting inorganic flocculant into the precipitation reactor.

4. Conclusions

Our experimental results confirm that rapid removal of radioactive Cs from waste seawater under emergency conditions can be achieved by applying nanochabazite. The high reactivity of the nanoparticles already recognized in chemical reactions (Hochella et al., 2008; Navrotsky et al., 2008) might also be useful in the engineering field of treatment processes for radioactive wastewater. The extremely fast adsorption rate of contaminants achieved by the nanoparticulate zeolite has not been observed with bulk materials. The nanochabazite reached an adsorption equilibrium state within 1 min. We demonstrated Cs adsorption by

nanochabazite at reaction rates that are of orders of magnitude higher than those of larger chabazite phases. The positive correlation between the rate constant ratio between them ($k_{2,bulk}/k_{2,nano}$) and the different initial Cs concentrations was observed with a correlation coefficient of 0.99. Our results also demonstrated that the nanozeolite could be easily precipitated from the high-salt solution immediately after cesium adsorption and the particle precipitation could be enhanced by the addition of ferric flocculant. The flocculation index reached a steady state within 10 min. To fully develop this novel and innovative approach to hazardous waste treatment, extensive studies on the application of nanomaterials should be encouraged.

Acknowledgments

This work was supported by the National Research Foundation of Korea (NRF) grant funded by the Korea government (MSIP) (No. NRF-2012M2A8A5025658).

References

Ahn, M.K., Iton, L.E., 1991. Solid-state cesium-133 NMR studies of cations in Cs/Li/Na Zeolite A: an example of cation dynamics involving three sites. J. Phys. Chem. 95, 4496–4500.

ANS report, 2012. FUKUSHIMA DAIICHI: ANS Committee Report. http://fukushima.ans.org/report/Fukushima_report.pdf.

Bosch, J., Lee, K.Y., Jordan, G., Kim, K.W., Mechenstock, R.U., 2012. Anaerobic, nitrate-dependent oxidation of pyrite nanoparticles by *Thiobacillus denitrificans*. Environ. Sci. Technol. 46, 2095–2101.

Bourgogne, M., Guth, J.L., Wey, R., 1985. US patent, No. 4, 4503,024.

Bratby, J., 2006. Coagulation and Flocculation in Water and Wastewater Treatment. IWA Publishing, London.

Choi, S.Y., Lee, Y.J., Park, Y.S., Ha, K., Yoon, K.B., 2000. Monolayer assembly of zeolite crystals on glass with fullerene as the covalent linker. J. Am. Chem. Soc. 122, 5201–5209.

Cundy, C.S., Cox, P.A., 2005. The hydrothermal synthesis of zeolites: precursors, intermediates and reaction mechanism. Microporous Mesoporous Mater. 82, 1–78.

Dubourg, M., 1998. Review of advanced methods for treating radioactive contaminated water. Radioprotection 33, 35–46.

Hedlund, J., Schoeman, B., Sterte, J., 1997. Ultrathin oriented zeolite LTA films. Chem. Commun. 13, 1193–1194.

Ho, Y.S., McKay, G., 1998. Sorption of dye from aqueous solution by peat. Chem. Eng. J. 70, 115–124.

Hochella, M.F., Lower, S.K., Maurice, P.A., Penn, R.L., Sahai, N., Sparks, D.L., Twining, B.S., 2008. Nanominerals, mineral nanoparticles, and Earth systems. Science 319, 1631–1635.

Jawor, A., Hoek, E.M.V., 2010. Removing cadmium ions from water via nanoparticle-enhanced ultrafiltration. Environ. Sci. Technol. 44, 2570–2576.

Kim, K.W., Lee, K.Y., Baek, Y.J., Chung, D.Y., Lee, E.H., Moon, J.K., 2015. Evaluation of the stability of precipitated uranyl peroxide and its storage characteristics in solution. J. Nucl. Sci. Technol. http://dx.doi.org/10.1080/00223131.2015.1038662.

Kosaka, K., Asami, M., Kobashigawa, N., Ohkubo, K., Terada, H., Kishida, N., Akiba, M., 2012. Removal of radioactive iodine and cesium in water purification processes after an explosion at a nuclear power plant due to the Great East Japan Earthquake. Water Res. 46, 4397–4404.

Mahmoud, D.K., Mohd Salleh, M.A., Wan Abdul Karim, W.A., Idris, A., Abidin, Z.Z., 2012. Batch adsorption of basic dye using acid treated kenaf fibre char: equilibrium, kinetic and thermodynamic studies. Chem. Eng. J. 181–182, 449–457.

Mengual, O., Meunier, G., Cayre, I., Puech, K., Snabre, P., 1999. Characterisation of instability of concentrated dispersions by a new optical analyser: the Turbiscan MA 1000. Colloids Surf. A – Physicochem. Eng. Aspects 152, 111–123.

Mimura, H., Kanno, T., 1985. Distribution and fixation of cesium and strontium in zeolite A and chabazite. J. Nucl. Sci. Technol. 22, 284–291.

Navrotsky, A., Mazeina, L., Majzlan, J., 2008. Size-driven structural and thermodynamic complexity in iron oxides. Science 319, 1635–1638.

Nilchi, A., Saberi, R., Moradi, M., Azizpour, H., Zarghami, R., 2011. Adsorption of cesium on copper hexacyanoferrate – PAN composite ion exchanger from aqueous solution. Chem. Eng. J. 172, 572–580.

Pan, Y., Ju, M., Yao, J., Zhang, L., Xu, N., 2009. Preparation of uniform nano-sized zeolite A crystals in microstructured reactors using manipulated organic template-free synthesis solutions. Chem. Commun. 46, 7233–7235.

Pendergast, M.M., Hoek, E.M.V., 2011. A review of water treatment membrane nanotechnologies. Energy Environ. Sci. 4, 1946–1971.

Plazinski, W., Rudzinski, W., 2009. Modeling the effect of surface heterogeneity in equilibrium of heavy metal ion biosorption by using the ion exchange model. Environ. Sci. Technol. 43, 7465–7471.

Qu, X., Alvarez, P.J.J., Li, Q., 2013. Applications of nanotechnology in water and wastewater treatment. Water Res. 47, 3931–3946.

Reddad, Z., Gerente, C., Andres, Y., Le Cloirec, P., 2002. Adsorption of several metal ions onto a low-cost biosorbent: kinetic and equilibrium studies. Environ. Sci. Technol. 36, 2067–2073.

Ridha, F.N., Yang, Y., Webley, P.A., 2009. Adsorption characteristics of a fully exchanged potassium chabazite zeolite prepared from decomposition of zeolite Y. Microporous Mesoporous Mater. 117, 497–507.

Sangwal, K., 2007. Additive and Crystallization Processes: from Fundamentals to Applications. John Wiely & Sons Ltd., West Sussex, England.

Serrano, D.P., Aguado, J., Morales, G., Rodríguez, J.M., Peral, A., Thommes, M., Epping, J.D., Chmelka, B.F., 2009. Molecular and meso- and microscopic properties of hierarchical nanocrystalline ZSM-5 zeolite prepared by seed silanization. Chem. Mater. 21, 641–654.

Sharma, Y.C., Srivastava, V., Singh, V.K., Kaul, S.N., Weng, C.H., 2009. Nano-adsorbents for the removal of metallic pollutants from water and wastewater. Environ. Technol. 30, 583–609.

Smith, L.J., Eckert, H., Cheetham, A.K., 2001. Potassium cation effects on site preference in the mixed cation zeolite Li, Na-Chabazite. Chem. Mater. 13, 385–391.

Subotic, B., Bronic, J., 2003. Handbook of Zeolite Science and Technology. Marcel Dekker, New York.

Sylvester, P., Milner, T., Jensen, J., 2013. Radioactive liquid waste treatment at Fukushima Daiichi. J. Chem. Technol. Biotechnol. 88, 1592–1596.

TEPCO report, 2011. Storage and Treatment Plan for the Water Containing High-level Radioactive Materials at Fukushima Daiichi Nuclear Power Station. http://www.tepco.co.jp/en/press/corp-com/release/betu11_e/images/110603e12.pdf.

TEPCO report, 2012a. A One-year Review of Fukushima Daiichi Nuclear Power Station "Steps to Achieve Stabilization". http://www.tepco.co.jp/en/nu/fukushima-np/images/handouts_120311_03-e.pdf.

TEPCO report, 2012b. Nuclides Analysis Results of Water at Water Treatment Facility. http://www.tepco.co.jp/en/nu/fukushima-np/images/handouts_120326_08-e.pdf.

Tsai, S.C., Wang, T.H., Wei, M.H., Teng, S.P., 2009. Cesium adsorption and distribution onto crushed granite under different physicochemical conditions. J. Hazard. Mater. 161, 854–861.